Physics in Medicine & Biology

IPEM Institute of Physics and Engineering in Medicine

PAPER • OPEN ACCESS

# A proof-of-concept of cross-luminescent metascintillators: testing results on a BGO:$BaF_2$ metapixel

To cite this article: G Konstantinou *et al* 2023 *Phys. Med. Biol.* **68** 025018

IOP Publishing Phys. Med. Biol. 68 (2023) 025018 https://doi.org/10.1088/1361-6560/acac5f

Physics in Medicine & Biology

IPEM Institute of Physics and Engineering in Medicine

OPEN ACCESS

RECEIVED
8 July 2022

REVISED
6 December 2022

ACCEPTED FOR PUBLICATION
16 December 2022

PUBLISHED
11 January 2023



PAPER

# A proof-of-concept of cross-luminescent metascintillators: testing results on a BGO:$BaF_2$ metapixel

**G Konstantinou**[1,2,*], **R Latella**[1,2], **L Moliner**[2], **L Zhang**[1], **J M Benlloch**[2], **A J Gonzalez**[2] and **P Lecoq**[1,2]

[1] Multiwave Metacrystal S.A., 34 Route de la Galaise, 1228, Geneva, Switzerland
[2] Instituto de Instrumentación para Imagen Molecular (I3M), Centro Mixto CSIC—Universitat Politècnica de València, 46022 Valencia, Spain
[*] Author to whom any correspondence should be addressed.

**E-mail:** georgios@metacrystal.ch

**Keywords:** positron emission tomography, instrumentation, front-end detector, scintillation, metascintillators

## Abstract

*Objective*: Time-of-flight positron emission tomography (PET) is the next frontier in improving the effective sensitivity. To achieve superior timing for time-of-flight PET, combined with high detection efficiency and cost-effectiveness, we have studied the applicability of BaF2 in metascintillators driven by the timing of cross-luminescence photon production. *Approach*: Based on previous simulation studies of energy sharing and analytic multi-exponential scintillation pulse, as well as sensitivity characteristics, we have experimentally tested a pixel of 3 × 3 × 15 mm3 based on 300 $\mu$m BGO and 300 $\mu$m BaF2 layers. To harness the deep ultraviolet cross-luminescent light component, which carries improved timing, we use the FBK VUV SiPM. Metascintillator energy sharing is addressed through a double integration approach. *Main results*: We reach an energy resolution of 22%, comparable to an 18% resolution of simple BGO pixels using the same readout, through the optimized use of the integrals of the metascintillator pulse in energy sharing calculation. We measure the energy sharing extent of each pulse with a resolution of 25% and demonstrate that experimental and simulation results agree well. Based on the energy sharing, a timewalk correction is applied, exhibiting significant improvements for both the coincidence time resolution (CTR) and the shape of the timing histogram. We reach 242 ps CTR for the entire photopeak, while for a subset of 13% of the most shared events, the CTR value improves to 108 ps, comparable to the 3 × 3 × 5 mm3 LYSO:Ce:Ca reference crystal. *Significance*: While we are considering different ways to improve further these results, this proof-of-concept demonstrates the applicability of cross-luminescence for metascintillator designs through the application of VUV compatible SiPM coupling, and easily implementable digital algorithms. This is the first test of $BaF_2$-based metascintillators of sufficient stoppng power to be included in a PET scanner, demonstrating the industrial applicability of such cross-luminescent metascintillators.

## 1. Introduction

One of the most important techniques in molecular imaging is positron emission tomography (PET). This modality is based on detecting two gamma photons resulting from the e+-e- annihilation of an emitted positron. Time-of-flight (TOF) information narrows the position of annihilation along the Line of Response (LOR) that joins the detection position of the two annihilation photons. Data with TOF improves the PET image's statistical properties and the signal-to-noise ratio (SNR) (Konstantinou *et al* 2021a). Currently, the best TOF resolution in commercial PET systems is 213 ps (Carlier *et al* 2020). The concept of meta-scintillators arises with the aim to improve this TOF without worsening other parameters (Lecoq 2017).

We can define as meta-scintillators the composite topologies of scintillating and light-guiding materials arranged to produce a synergistic effect in the scintillation process, combining thus the favorable physical characteristics of their constituting components. The efforts in this direction are intended to provide the basis

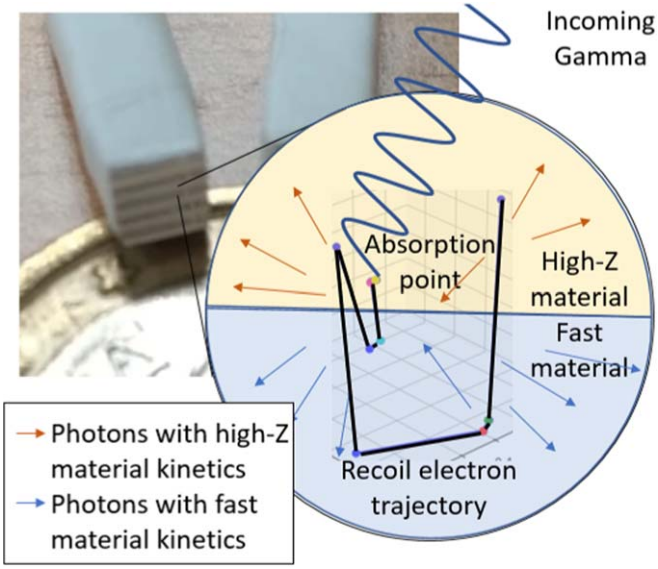


**Figure 1.** First-generation metascintillator conceptual design, demonstrating the process of energy being leaked into the fast material (blue) for gamma interactions taking place in the dense, high-Z material (yellow) through the simulated range of the recoil electron (black line). The orange arrows represent the slow and blue arrows the fast isotropic production of photons.

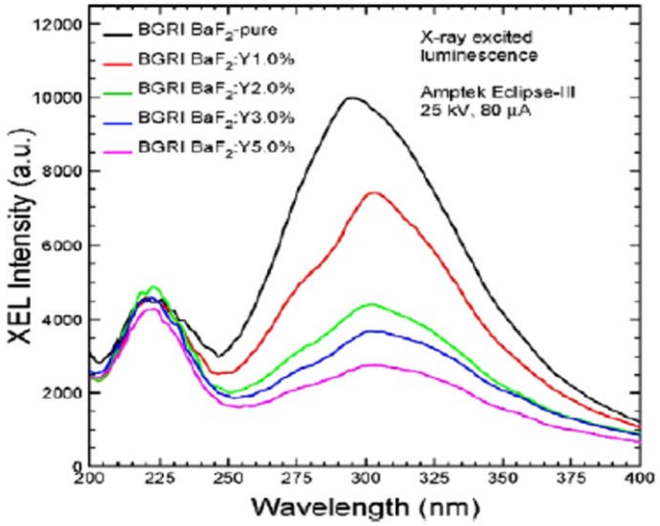


**Figure 2.** Slow component suppresion for pure $BaF_2$ different dopant concentration, in the wavelengths above 240 nm (Hu *et al* 2022).

for future developments that can lead to a TOF PET detector with sufficient gamma detection efficiency combined with a timing resolution in the order of 10 ps over the next years. This, although extremely challenging, is not limited by physical barriers (Lecoq *et al* 2020).

One way to combine the favorable characteristics of different scintillators is by finding a way in which they share the energy of each gamma interaction. It is possible to use a high-Z material benefiting from its stopping power and design an architecture that brings fast optical photon emitters in proximity, increasing the probability of recoil electrons crossing through them (Loignon-Houle *et al* 2022). Thus, some optical photons will be produced according to the favorable kinetics of the second, so-called fast material. Based on this concept, one possible meta-structure design is based on two scintillation components. One with improved high-Z (host) and a second with capabilities for fast emitter photons. They would be split into layers with thicknesses of less than the recoil electron range (around 500 $\mu$m for dense inorganic scintillators) and in an alternating arrangement (see figure 1). This constitutes the first tested and materialized generation of metascintillators.

In previous works, some designs used organic compounds such as the BC-422 (Saint-Gobain, France) and EJ232 (Eljen technologies, USA) as the fast emitter material (Lecoq *et al* 2022). However, organic scintillators have significantly lower stopping power than inorganic ones. This leads to a meta-structure design that might

demonstrate significant improvements in timing but at the cost of reducing stopping power. Due to the nature of the PET technique based on the coincided detection of two particles, reducing sensitivity capabilities is not the optimal direction. Nevertheless, plastic-based metascintillators can be designed with a stopping power comparable to that of commercial designs if the volume ratio between the high-Z and fast materials is beyond 3:1. However, the amount of energy in the fast material is progressively reduced. To further increase the probability of energy sharing while retaining high efficiency, a material with sufficient stopping power and enough fast photon production needs to be considered.

Barium Fluoride ($BaF_2$) is a scintillator that allows cross-luminescence photons at around 200 nm to be produced and extracted because of its good transparency in the ultraviolet (UV) region (Gundacker *et al* 2021). $BaF_2$ combines a self-trapped excitonic scintillation with a decay component of around 600 ns (light yield of approximately 10 000 photons per MeV), with an optical cross-luminescence component with a fast decay of 0.6 ns and 1800 photons per MeV. The precise nature of the scintillation mechanism responsible for the two deep-UV components is still under study. However, the advantage of these fast components in timing is unambiguous. While the fast cross-luminescence component can provide superior timing (Lecoq *et al* 2022), it isn't easy to detect as its wavelength is between 170 and 220 nm, in contrast with the slow component with a higher wavelength peak at around 310 nm (see figure 2). $BaF_2$ is not hydroscopic, but condensing moisture can pit its surface. $BaF_2$ has a density of 4.88 g $cm^{-3}$ and a better radiation length than organic scintillators (2.05 cm) (Zhu 1994). Therefore, it provides substantial stopping power for PET applications, even though not enough to compare with state-of-the-art materials such as BGO (radiation length 1.12 cm) or LYSO (radiation length 1.2 cm) (Mao *et al* 2011, Saint 2021). Nevertheless, combining such scintillators with $BaF_2$ leads to an effective radiation length between these values, becoming attractive for metascintillation structures.

As the slow component of $BaF_2$ has a rather long decay time, it is not relevant for timing applications but can be used for energy determination. However, the long decay can lead to pulse pile-up and thus, increase the dead-time of a $BaF_2$ detector. For this reason, different dopants (e.g. Yttrium, Cadmium fluoride, and Lanthanum trifluoride) have been applied to suppress this part of the pulse (figure 2) (Hu *et al* 2022).

Concerning the photon detection of the deep-UV fast component, recent developments in SiPM technology (Capasso *et al* 2020, Ieki *et al* 2019) provide the possibility to detect these photons with up to 22% photon detection efficiency. Both FBK (Italy) and Hamamatsu Photonics (Japan) have developed SiPMs to support liquid argon and liquid xenon-based detectors used in high-energy physics, for instance, in the search for dark matter. This technical development now renders $BaF_2$-based radiation detectors as potential candidates for TOF PET applications.

In this work, we report the first results on a BGO:$BaF_2$ metascintillator, structured in a pixel configuration with a 1:1 volume ratio between the two materials. We explain the reasons why this particular design, dimensions, and characteristics were chosen; the simulations used to foresee the timing and energy sharing behavior; the agreement between simulation and experimental measurements; the analysis pursued to isolate and separate photoelectric interactions and fast events; and finally, the timing characteristics of a dense, easy to build metascintillator that can form the backbone for the first system-level designs to be pursued on this direction. All this is presented to demonstrate how the complexity of interactions between the two materials and the optical coupling to an ultraviolet-sensitive SiPM constitute an optical circuit for the gamma detection application.

## 2. Materials and methods

### 2.1. Metascintillators assembly

In previous works, we have explained in detail the process of simulations based on metascintillators (Konstantinou *et al* 2020). We first perform a series of simulations using GATE 8.2, a GEANT4-based Monte Carlo platform (Jan *et al* 2004). In each of them, the analyzed metascintillator consists of periodic alternating layers of the two scintillation materials with different thicknesses, illuminated by 10M 511 keV gamma rays (Moliner *et al* 2021). This structure has already been tested in previous works, and the main characteristic is the easiness of construction. This simulation does not include optical photon production to reduce the computational load.

Thus, we obtained relevant information on the traits expected from a testable meta-structure. $BaF_2$, unlike organic compounds, leads to a large average energy sharing, with a peak in the distribution at around 320 keV for photoelectric interactions (figure 3). To be noted, this is not any sort of photopeak; this value merely demonstrates the most likely value of energy sharing for events interacting through photoelectric or fully contained Compton interactions. In practice, this corresponds to the highest likelihood of shared events being that 320 keV are released in BGO, and the rest 191 keV in $BaF_2$. Apart from that, a population of events only interacts with BGO, corresponding to the peak at 0 keV, and another population of events directly interacts with

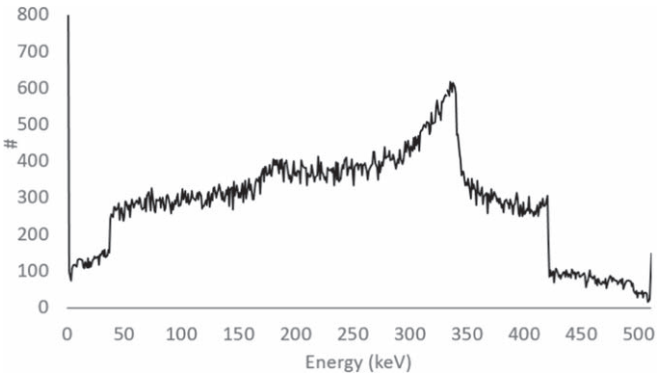


**Figure 3.** Energy sharing through the energy released in the fast emitter for 511 keV interactions, as seen in Monte Carlo simulation of a 300 $\mu$m BGO- 300 $\mu$m $BaF_2$ metapixel. Notice the peaks at 0 (fully BGO) and 511 keV (fully $BaF_2$), along with the sharing distribution peaking around 320 keV.

**Figure 4.** Photo of a 300 $\mu$m BGO- 300 $\mu$m $BaF_2$ metapixel of total dimensions $3 \times 3 \times 15$ $mm^3$. The difference in color and refractive index between the two materials is directly visible as a change in shade.

$BaF_2$ with all energy being retained without any leakage to BGO. This corresponds to the sharp peak at 511 keV, at the right end of the figure 3 plot. The visible features within the plot are related to the energy of bound states of the heavier nuclei in the crystal structures of BGO and $BaF_2$. For instance, the step at 37 keV corresponds to 474 keV K-shell photoelectron energy of barium, while the one at 420 keV with the same of Bismouth. This plot corresponds to the energy absorbed in the $BaF_2$, for 511 keV gammas fully absorbed by the system; the complementary energy has been absorbed in BGO.

To confirm the simulations and benchmark the performance of $BaF_2$-based meta-structures, we have developed a pixel-shaped metascintillator (metapixel). This metapixel has dimensions of $3 \times 3 \times 15$ $mm^3$ and provides enough sensitivity on a 1-to-1, single SiPM setup for coincidence time resolution (CTR) measurements. The exact volume ratio and slab dimension have been determined on the one hand from the simulation results on energy sharing and expected effective radiation length of the resulting meta-structure, and on the other hand, from the material characteristics, cost, and ease of use. With these considerations in mind, the metapixel to be tested is composed of 10 pieces, 5 of BGO (EPIC crystals, China) and 5 of $BaF_2$ (SICCAS, China) of $3 \times 15$ $mm^2$ area and 300 $\mu$m thickness, of all-sides-polished, see figure 4. The metascintillator was then wrapped in Teflon.

### 2.2. Test setup

The metapixels were measured against a 3 x 3 x 5 $mm^3$ LYSO:Ce:Ca (SIPAT, China) reference crystal, read out with a $3.4 \times 3.9$ $mm^2$ NUV SiPM with $40 \times 40$ $\mu m^2$ cell sizes from FBK. The crystal has been optically coupled to the SiPM using optical grease of 1.6 refractive index (RI). The SiPM readout circuit includes a high bandwidth timing channel based on a balun transformer, radiofrequency amplifiers and a standard energy channel with a bandwidth less than 1 GHz. This reference detector has been determined to have 78 ps (FWHM) detector timing resolution (Latella *et al* 2021).

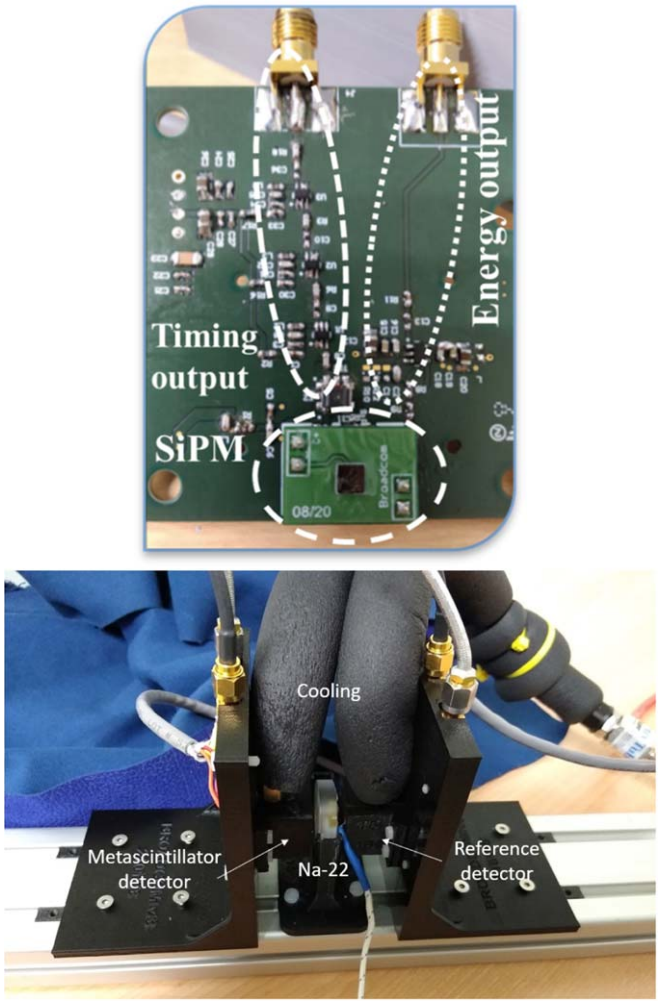


**Figure 5.** (top) SiPM circuit with two channels, compatible with both NUV and VUV SiPMs form FBK; and (bottom) coincidence test setup, including compressed air cooling.

While the high bandwidth allows this setup to perform significantly better and closer to the experimental state of the art, environmental factors such as the lack of electromagnetic shielding and limited temperature stabilization lead to coincidence timing measurements somewhat closer to realistic, deployable and scalable electronics.

The same circuit is used for the metapixel, however the SiPM used was a $3.0 \times 3.4$ mm$^2$ VUV SiPM with $35 \times 35$ $\mu$m$^2$ cell size also from FBK. Given that ultraviolet sensitivity is necessary and most commercial optical grease compounds are opaque for these wavelengths, we used glycerin. Pure glycerin has a melting point of 13.3 °C, which lowers with an increasing concentration of water or other solvents. Our tests are performed at a constant temperature of around 10 °C.

Using cooling for this test is not only related to the condition of the glycerine; temperature stabilization is required for any SiPM application focused on timing, as when high overvoltage is applied, all specifications of the readout are sensitive to minor temperature variations. In particular, the gain of the SipM changes in the order of 1% per °C. For this reason, cooling also needs to be included in every PET system.

While the high bandwidth allows this setup to perform significantly better and closer to the experimental state of the art, environmental factors such as the lack of electromagnetic shielding and limited temperature stabilization lead to coincidence timing measurements somewhat closer to realistic, deployable and scalable electronics. Retaining a temperature below 12 °C. and with $\pm 3$ °C. variation does not constitute a significant complication of the standard temperature stabilization approach in deployed PET scanners.

The two detectors were tested in coincidence using an encapsulated source of Na-22, with an activity of 12 uC and an active diameter of 0.25 mm, placed centered in between the detectors (figure 5). Each channel signal is digitalized using a Rode Schwarz RTP084 high-performance oscilloscope with 8 GHz bandwidth, at a sampling rate of 100 Gsps.

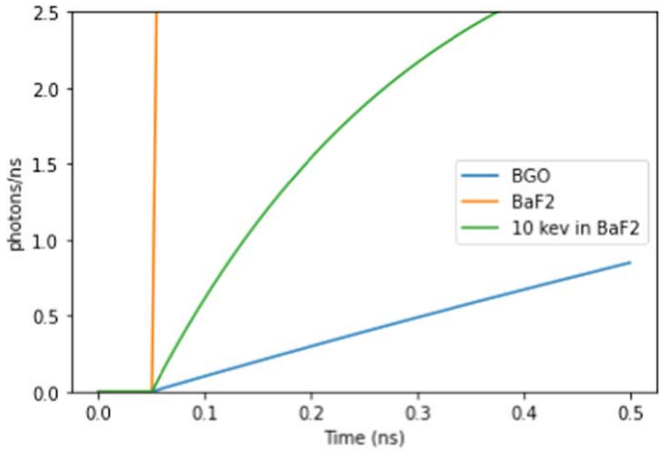


**Figure 6.** First half nanosecond of photon/ns rate of events according to the hex-exponential model, for 0, 10 and 511 keV in $BaF_2$. Note the expected slope diference, even when a small amount of energy is leaked to the fast emitter.

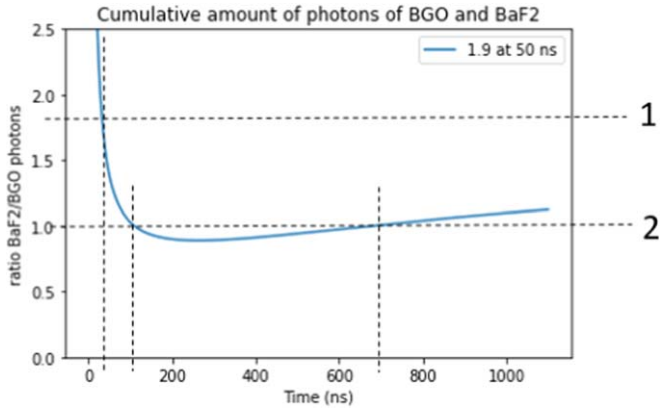


**Figure 7.** Cumulative amount of photons as a ratio of $BaF_2$ over BGO. Integration windows where the measurement is insensitive to energy sharing (dashed line 2) are found where the two quantities are equal and ratio equals to 1. In contrast, around 50 ns from event onset, the ratio is close to 2, allowing for energy-sharing dependent discrimination (dashed line 1).

### 2.3. Analytic multi-exponential model and simulations

We performed a detailed analysis of the expected pulse characteristics based on the known photon production time-series, SiPM characteristics and readout circuit performance limitations. As previous works (Konstantinou, *et al* 2020) described, unlike conventional scintillators, metascintillators have a quad-exponential photon production time-series. Cross-luminescent metascintillators have a hex-exponential (corresponding to six different exponential components) photon production time-series: a standard bi-exponential for each detector and the separate fast component of $BaF_2$ (equation (1)):

$$f_{ms}(t) = PDE_{BGO}\frac{E_{BGO}\times LY_{BGO}}{\tau_{dBGO}-\tau_{rBGO}}(e^{-\frac{t}{\tau_{dBGO}}}-e^{-\frac{t}{\tau_{rBGO}}}) + PDE_{BaF_2f}\frac{E_{BaF_2}\times LY_{BaF_2}}{\tau_{dBaF_2f}-\tau_{rBaF_2f}}(e^{-\frac{t}{\tau_{dBaF_2f}}}-e^{-\frac{t}{\tau_{rBaF_2f}}}) + PDE_{BaF_2s}\frac{E_{BGO}\times LY_{BGO}}{\tau_{dBaF_2s}-\tau_{rBaF_2s}}(e^{-\frac{t}{\tau_{dBaF_2s}}}-e^{-\frac{t}{\tau_{rBaF_2s}}}), \quad (1)$$

where $E$ is the released energy, $LY$ the light yield, PDE the average photon detection efficiency for the emission wavelengths, $\tau_d$ the decay coefficient, $\tau_r$ the rise coefficient; BGO subscripts correspond to BGO characteristics, $BaF_2f$ to the fast component and $BaF_2s$ to the slow component of $BaF_2$.

From analyzing this hex-exponential function, we demonstrate the significant improvement of event onset-photon arrival $\Delta$t between photoelectric interactions in BGO and BaF2 and even for only 10 keV being leaked to the $BaF_2$ (figure 6). This information is significant in support of an energy-sharing timewalk correction.

In more recent publications, it has been found that apart from the dominant decay components in crystals such as BGO and $BaF_2$, other ultrafast components with smaller and sometimes marginal participation can be

isolated (Gundacker *et al* 2020). While such components could indeed alter the understanding of early photon density, the main purpose of this figure is to demonstrate that even a small amount of energy in the fast scintillator, can significantly alter the characteristics of the pulse at the onset. In fact, taking into account the statistical character of arrival of the first photons, the multi-exponential model should be carefully applied, if one wants to study the beginning of the pulses. Other more complex analytic approaches could provide a better fit, focusing on initial photon time density (Mohr *et al* 2022).

### 2.4. Double integral approach

We analyzed the integral of the hex-exponential expression, which, as a time-series function, corresponds to the pulse's integral for increasing duration integration windows. This is of particular interest since integration windows where the pulse energy measurement is insensitive to energy sharing can be thus detected (Konstantinou *et al* 2021b). Similarly, integration windows where the energy measurement is significantly affected by the extent of energy sharing, can be useful as surrogate measurements for estimating it. The ratio of integrals of the two components of equation (1) is plotted in figure 7. From this plot, we see that an integral window around 50 ns after event onset provides a ratio of prompt over slow photon emission up to 1.9, when the pulse is fully released in $BaF_2$. In contrast to this, at around 90 ns and 670 ns, the measurement is insensitive to energy sharing.

This tool serves as a guideline to support the choice of photoelectric interactions on the experimental dataset and enhance our understanding of the measurements. To improve the energy resolution of the system, we optimize the energy measurement $E_{cor}$ as a weighted linear combination of 50 ns and 670 ns integrals, compensating for uncertainties in the light yield, PDE, bandwidth and other characteristics (equation (2)). The 670 ns window was chosen as the higher number of photons collected improves the energy resolution, compared to the 90 ns window.

$$E_{cor}(E_{\mathrm{BGO}},\ E_{\mathrm{BaF_2}}) = \int_0^{670\ ns} f_{ms}(t)dt - w\int_0^{50\ ns} f_{ms}(t)dt. \tag{2}$$

The uncertainty of defining the precise value of energy sharing is termed energy sharing resolution and corresponds to a calculated FWHM of the energy sharing histogram, more easily retrieved at the extremes of BGO-only and $BaF_2$-only events.

All energy measurements, either to define energy resolution or to estimate the energy sharing spectrum were performed using pulse integration. While in single scintillators the maximum value of the pulse corresponds roughly to the energy of interaction, in metascintillators it corresponds to a combination of energy of interaction and energy sharing. As such, it cannot be used for energy measurements. For the Gaussian fit of the photopeak, the area within 2 sigma of the maximum value was used.

For the present analysis we also used a BGO pixel of $3 \times 3 \times 15\ mm^3$, to be able to compare the characteristics of metascintillator pulses with those of a more well-known material. This pixel was wrapped in Teflon, having all surfaces polished and coupled to the photodetector using glycerine to compare the BGO signal obtained in the same conditions as for the BGO:BaF2 metapixel.

### 2.5. Timewalk correction

As can be deduced from the model demonstration in figure 6, the difference in time between event onset and first photon detection is strongly influenced by the amount of energy sharing. In timing studies, we usually focus on the statistical uncertainty of detection, which is reflected in the CTR value. However, in metascintillators, if we plot the delta tau distributions of event subsets, defined by the extent of energy sharing, we also see a shift in the mean value (Konstantinou *et al* 2021b). In this sense, if he extent of energy sharing is detectable, the measured value can be corrected for each single event, in an energy-sharing-dependent timewalk correction.

### 2.6. Gamma sensitivity calculation

According to Beer's law (equation (2)), a gamma impinging the scintillator has a finite probability $P_{int}$ of interacting with it, depending on the scintillatior's length $x$ and gamma attenuation or radiation length $\lambda_{att}$. In the case of metascintillators, the area ratio of the components $A$ adds a second statistical dependency related to which material the gamma is likely to imping on. In this sense, the Beer law for metascintillators is transformed into the complex form of equation (3). Particularly for the pixel under test, this form leads to equation (4). Once this equation has been calculated, it is possible to reverse equation (2) and reach a value of effective radiation length for metascintillators $\lambda_{eff}$. We compare this metascintillator with BGO, LYSO and $BaF_2$ of the same 15 mm length

$$P_{int}(x) = 1 - e^{\frac{-x}{\lambda_{att}}} \tag{3}$$

$$P_{int}(x) = 1 - (A_1 e^{\frac{-x}{\lambda_{att1}}} + (1 - A_1)e^{\frac{-x}{\lambda_{att2}}}) = 1 - e^{\frac{-x}{\lambda_{eff}}} \tag{4}$$

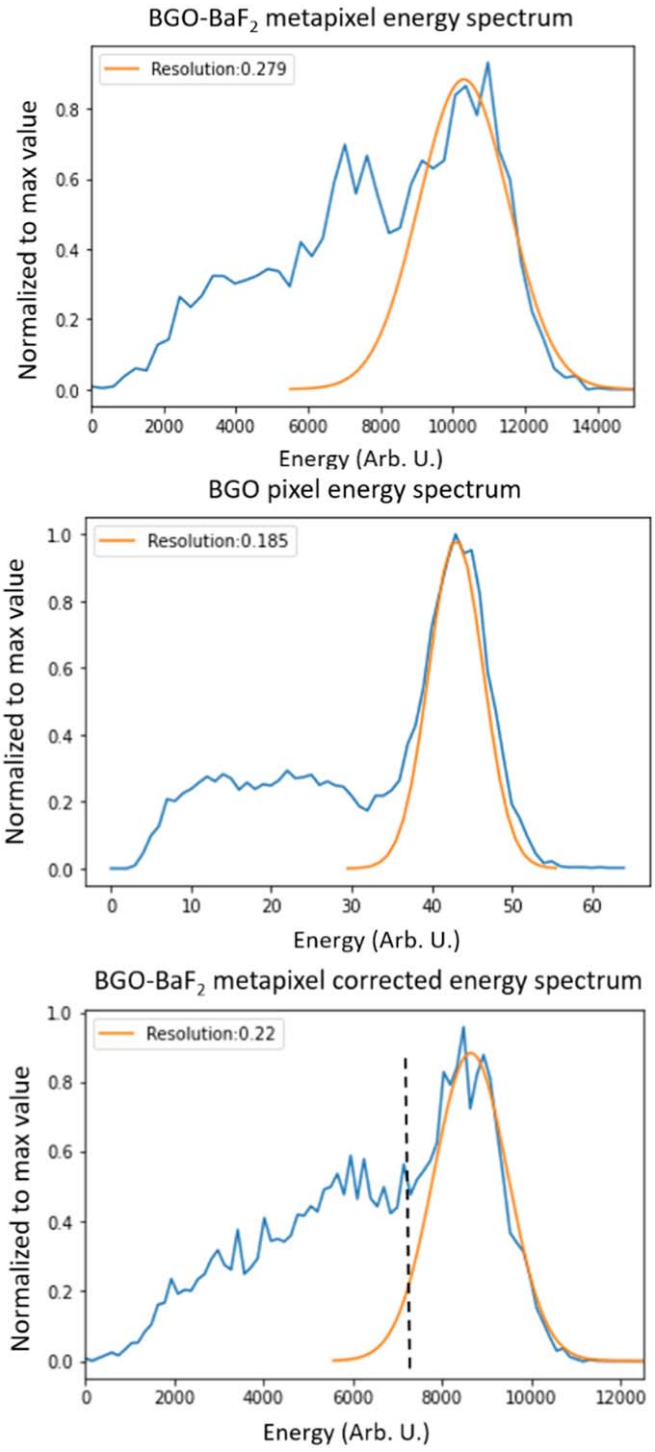


**Figure 8.** (top) Energy histogram of a $3 \times 3 \times 15$ mm$^3$ BGO pixel , measured with VUV SiPM; (midde) Energy histogram of the BGO:$BaF_2$ metapixel, at best projected integration window; and (bottom) Energy histogram of the BGO:$BaF_2$ metapixel corrected through the use of the second integral. The dashed line corresponds to the threshold used to define the photopeak. Y-axis corresponds to histogram normalized on the maximum value.

$$P_{int\,\mathrm{BGO-BaF_2}}(x) = 1 - \left(\frac{1}{2}e^{\frac{-x}{\lambda_{att\,\mathrm{BGO}}}} + \frac{1}{2}e^{\frac{-x}{\lambda_{att\,\mathrm{BaF2}}}}\right). \quad (5)$$

## 3. Results

### 3.1. Energy resolution of the detector

Figure 8 top shows that the energy profile using the VUV SiPM with a $3 \times 3 \times 15$ mm$^3$ BGO results in a photopeak with a resolution of 18.5%. When we test the metapixel, the resolution is almost 28% (figure 8

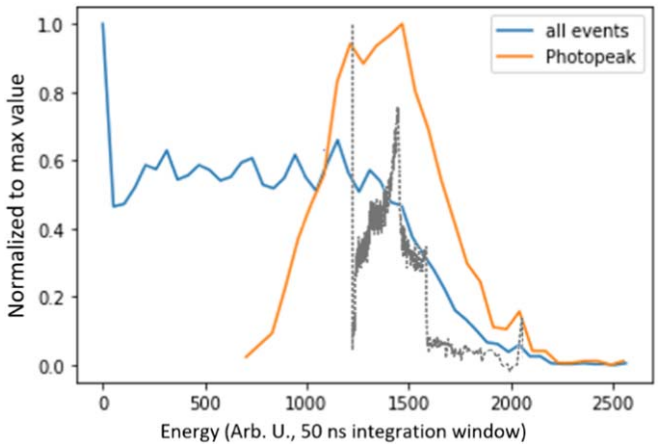


**Figure 9.** Energy histogram (blue) of BGO:$BaF_2$ metapixel, for a short window (50 ns). Overlayed, the events belonging to the photopeak (orange) as qualified by the histogram of figure 8 (bottom). On that dataset, we overlay the simulated energy sharing distribution (black-dotted) from figure 4, in exponential scale to reflect the relation between energy sharing and photon population. The peak around 2050 represents photoelectric events where the energy is fully released in $BaF_2$, while the peak around 1200 corresponds to photoelectric events where the energy is fully released in BGO.

middle). However, by applying the analytic approach of feature resolution optimization mentioned before (equation (2)), we can improve the energy spectrum of the metapixel enough to acquire an energy resolution of 22%, that is, an improvement of 21% compared to the simple integration window (figure 8 bottom). The optimal weight w was found to be 0.092. This resolution, albeit not ideal for system deployment, allows a clearer definition of the photopeak area. With a deeper understanding of the single-pixel system and parameters such as respective light yields, photon detection efficiencies, number of photons lost due to imperfect coupling or limited electronics bandwidth, it is expected that the energy resolution can be further improved.

### 3.2. Estimation of energy sharing

Different integration windows provide a clearly distinct photopeak (figure 8, bottom). If we choose the events belonging to it and refer to their energy at the short integration window, we get a distribution as shown in figure 9. This distribution has three distinguishable peaks, visible through and within the imperfect resolution of the feature, namely at $1200 \pm 50$ Arb. U., $1450 \pm 50$ Arb. U. and $2050 \pm 80$ Arb. U. We overlay the distribution of energy sharing as retrieved from simulation and shown in figure 3, but plotted exponentially along the $x$-axis. This is done as the number of photons received at this short integration window has an exponential relation to the value of energy sharing due to the bandwidth constraints of the slow channel. With this, these peaks correspond to the BGO-only, shared, and $BaF_2$-only events.

We estimate the feature resolution by measuring the FWHM of the rising slope at the BGO-only value, which corresponds to a single light yield. If we follow the same approach as energy resolution, we retrieve an energy sharing resolution of 25%. This is like the energy resolution of the detector. With this information, we show how the short integral approach can provide enough information on energy sharing to be used for timewalk correction and optimization of detector timing resolution.

### 3.3. Timewalk correction and CTR results

The $\Delta t$ distribution vs the reference for this easily isolated photopeak leads to an FWHM value of $319 \pm 13$ ps (figure 10 top). Compared to Gaussian, Laplacian, or Lorentzian, the distribution does not significantly match any of the three, as the best mean-square value $R^2$ is only 0.892.

We applied a 1st order linear correction on the arrival time recorded for the events belonging to the photopeak. With this application, we reach an FWHM value of 190.5 ps, with an $R^2$ value of 0.957 for a Lorentzian fit (figure 10 bottom). If we decouple the reference contribution, we reach an expected BGO:$BaF_2$ 1:1 volume ratio metapixel-metapixel CTR of $241.1 \pm 15$ ps. The corresponding CTR for BGO crystals in the same conditions was measured around $535 \pm 33$ ps. The roughness and bumps of the BGO event distribution could be caused by low statistics and lack of timewalk correction to take full advantage of the Cherenkov photon timing. All of the above FWHM values were retrieved directly from the dataset and not the fits, which tend to bias the result.

The energy sharing resolution of 25% does not allow confident isolation of BGO-only and shared subsets. This means that while timewalk correction is still applicable overall, the subsets themselves do not significantly improve the respective CTR values due to the high mixing of most events. In contrast, the secondary high peak

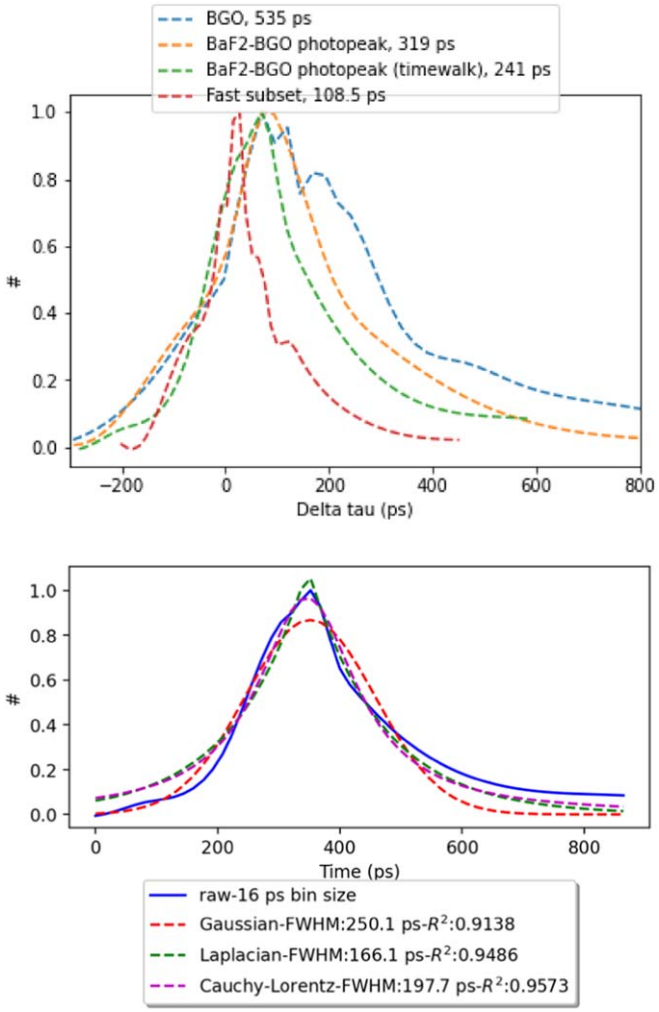


**Figure 10.** (Top) Delta Tau distributions leading to decoupled CTR measurements for BGO (535 ps), $BaF_2$:BGO metapixel without timewalk correction (319 ps), same with timewalk correction (242 ps) and fast subset (108.5 ps); and (bototm) comparing the timewalk corrected dataset with relevant fits, to understand the improvement by alligning the centroids of the different energy sharing subsets, as well as the variability of the bias due to different fitting functions.

on the right end of figure 10, at around 2050 Arb.U, is easily isolated. With an energy threshold corresponding to 1850 Arb.U. of that measurement, we separate the events with the highest amount of photons at 50 ns, which correspond to the highest energy sharing to $BaF_2$. This subset comprises 13% of the total events of the photopeak. By plotting the $\Delta$t distribution vs reference for these events, we reach a 109.4 ps FWHM. By considering the reference DTR, we have an equivalent 108.5 $\pm$8 ps metapixel-metapixel CTR (see red dashed line in figure 10 top). This means that the $3 \times 3 \times 15$ mm$^3$ BGO:$BaF_2$ metapixel has a marginally better temporal response for this subset of events, than the $3 \times 3 \times 5$ mm$^3$ LYSO:Ce:Ca reference crystal. Notice that the range of energy sharing in this dataset is relatively small, meaning that the number of fast photons detected does not significantly vary. As such, timewalk correction has not been applied in this subset.

### 3.4. Metascintillator sensitivity

In table 1 we show the results of applying the extended Beer law for the tested metapixel, along with standard scintillator references.

## 4. Discussion

This paper is reporting on the metascintillator analysis composed by BGO:$BaF_2$. Even though the two materials have distinct light yields, their small difference results in photopeaks found in the same area of the energy histogram, with only a small overlap of their Compton scatter areas.

The energy and energy sharing surrogate resolutions are in the order of 25–30%. This allows confident discrimination of 1 sigma around the photopeak. While the photopeak resolution after correction is not

**Table 1.** Sensitivity of different scintillating components.

| Scintillator | Radiation length (cm) | Gamma interaction % |
|---|---|---|
| $BaF_2$ | 2.05 | 51.9 |
| BGO | 1.12 | 83.2 |
| LYSO | 1.2 | 71.3 |
| **BGO:$BaF_2$** | **1.33** | **67.5** |

significantly different from BGO-only of the same size, there seems to be a poor differentiation between the photoelectric and Compton areas, partially caused by the significantly lower photo-fraction of $BaF_2$ and by the difference in the light yields of the two materials. For this calculation we use exclusively the two integrals already used to evaluate the energy sharing content of events. This allows simplicity in read-out, as two measurements per pulse are in par with modern system-level data acquisition systems (Binder *et al* 2021, Gómez *et al* 2022). The dead time of the detector is affected only by the length of $BaF_2$ pulse. While the longest integral we use is 670 ns, $BaF_2$ pulse lasts significantly more; this leads to a dead time close to 1.2 $\mu$s. This can be reduced by trivalent doping, such as $BaF_2$:Y, which quenches the slow component, while keeping the fast one unaffected (Hu *et al* 2022).

The first attempt of a linear timewalk correction deviates from the theoretical expectation that an exponential would fit better. Nevertheless, linear fitting seems to partially compensate for the uncertainty produced by limited energy sharing resolution. As such, at this stage, it is the best-case scenario; however, with improved energy resolution, the exponential time-walk is expected to improve further the fit of the timewalk and hence the CTR.

The use of glycerol at low temperatures poses technical difficulties. However, it still exhibits a good extraction of optical photons to the SiPM. The detector must remain in constant cooling, or glycerol melts, and has to be reapplied. Furthermore, liquid glycerol seems to gradually deteriorate the performance of the VUV SiPMs to a detrimental level. In extreme cases, a black dust, is found (figure 11). The reasons or mechanism of this are still under investigation. At the same time, the effect on functionality and lifetime is clear, as this is not easily adapted to an industrial-level development. Coupling materials with significant transparency in the VUV area are being researched, as well as solutions to improve the stability of VUV in the presence of glycerine.

This BGO:$BaF_2$ metapixel offers access to the energy-sharing information. However, they can only be studied using VUV SiPMs, while the possibility of better sensitivity in the VUV area by future SiPM designs can lead to further improvement of the timing characteristics of this metascintillator, with larger populations of fast photons being collected. At the moment, while the cost of both BGO and $BaF_2$ is only a fraction of the state-of-the-art material, LYSO (Lecoq *et al* 2022), the presented metapixel achieves similar timing and stopping power characteristics at the only cost of a slightly more complex readout scheme.

Having a mixed-signal scintillator which allows easy definition of a fast subset is similar to the case of Cherenkov timing (Kratochwil *et al* 2020). In this case, it is possible to determine coincidence pairs with variable CTR and use this information for reconstruction. In the best case scenario, ultra-fast pairs can be used as priors, with increased weight, allowing extra added value especially in clinical scenarios of low radiation. In particular, if we only consider these two possibilities, of fast (F) and standard events (S), coincidences can be fast-fast (FFC), standard-fast (FSC), or standard-standard (SSC). In table 2 we see that while FFC is reduced to a marginal number of events, FSC is a likely scenario, further improving the overall timing of the system. Analysis on the effective timing of mixed signal metascintillators is ongoing.

Cherenkov photons are also produced in the two crstal components of the metascintillator. Their improved timing is taken advantage of. Nevertheless, with these electronics, BGO, including Cherenkov, is measured to have a CTR around 500 ps. The discrepancy with the state of the art can be caused due to the fact that though we work with an optimized setup for timing, this setup is made to imitate realistic deployment conditions, rather than laboratory ones. This can be observed also by the CTR achieved with the reference detector, which is significantly larger than the same state of the art in the lab. Moreover, in the double integral approach, events with improved timing due to Cherenkov photons are grouped with the slow BGO ones and no particular time-walk correction is performed, to retrieve their improved timing. Finally, the acquisition took place using glycerine for coupling, to emulate the conditions of the metascintillator acquisition. In this sense, we expect that in future publications with optimal conditions, as long as BGO can demonstrate timing capabilities in the area of 300 ps, the metapixel will show a similar improvement in its CTR.

As these SiPM have mostly been designed with LYSO specifications in mind, the light yields of both $BaF_2$ and BGO are generally not leading to saturation. The same stands for the fast component of $BaF_2$, as even though initial photon time density is higher than that of LYSO, the low PDE of the SiPM at these wavelengths leads to reduced detection. In these senses, saturation correction on the SiPM is not necessary for this metascintillator.

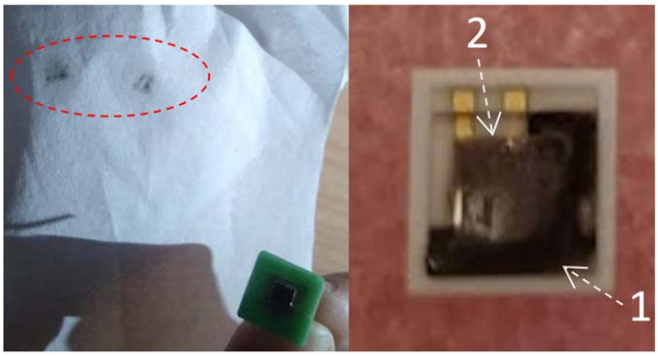


**Figure 11.** (left) residue (red circle) remaining after cleaning glycerol from FBK VUV SiPM samples; and (right) dirty Glycerol (1) leaking on the surface of Hamamatsu MPPC for cryogenic use/S13370 series (2) after use.

**Table 2.** BGO:$BaF_2$ metascintillator timing.

| Coincidence type | Coincidence percentage | Coincidence CTR |
|---|---|---|
| SSC | 75.6% | 241.2 ps |
| SFC | 22.7% | 187.0 ps |
| FFC | 1.7% | 108.5 ps |

The BGO:$BaF_2$ metapixel stands in the middle between BGO and $BaF_2$ in the sense of energy resolution and photofraction. The energy resolution is indeed worse than that of LYSO, but significantly better than that of $BaF_2$ by itself. Its sensitivity is similar to that of LYSO of same length. Nevertheless, given the measured value of BGO timing, the big advantage lies in reducing the overall CTR two-fold, leading to an overall increase of effective sensitivity for the system.

## 5. Conclusions

Further improvement on the electronics, including optimization for the energy measurement, can improve the reported characteristics. This will lead to both enhanced data collection and event subset separation. Currently, only two sets of events can be easily separated, general photopeak and ultra-fast. Those are sufficient for proof of concept but do not unleash the full potential of metascintillators, which relies on confidently determining how many fast photons have been produced per event to optimize the time-walk correction.

The double integral approach has been chosen for this proof-of-concept, as it is easily implementable in hardware and firmware. Other features, such as the rising slope or the maximum value of the pulse, could allow even better energy sharing resolution and event subset discrimination capabilities. This first attempt is only intended to set the basis for understanding how different pulse features can be combined to improve the performance of the metascintillator. The codes used for this analysis, enhanced with optimization and machine learning capabilities, are to be published as an open-source resource to generalize the use of metascintillators.

Apart from the standard $BaF_2$, similar metapixels are to be constructed and measured with doped variants, which suppress the slow component, improving the dead-time of the detector. The 300 $\mu$m dimension for the components is a compromise, as the simulation pointed at sufficient energy sharing, while construction and stability are also guaranteed. Thinner scintillator pieces have better energy-sharing characteristics but reduce the material utilization ratio during production and machining due to the increasing probability of being broken during cutting or polishing. Pieces of surface of $0.3 \times 3$ mm$^2$ have surface and cost similar to square pixels of $1 \times 1$ mm$^2$, which are commonly used in preclinical designs (Konstantinou *et al* 2020); such metapixel's dimensions are not unrealistic in the PET application in terms of either cost or number of independent scintillator pieces.

Concluding, in this publication, we report the first detailed results on a metapixel built and experimentally tested, based on BGO and $BaF_2$. The radiation length for this metapixel is calculated to be close to that of an LYSO crystal of the same length. We achieve an energy resolution of 22%, CTR of 241 ps, and for a subset of the events, an unprecedented 108.5 ps CTR. This is obtained for a scintillator of $3 \times 3 \times 15$ mm$^3$, which are realistic dimensions for system-level development.

## Acknowledgment

Part of the research presented in this manuscript was funded by the ERC grant "Innovative PET scanner for dynamic imaging", agreement no 695536. The concept presented in this manuscript was based on research first developed within the TICAL: 4D total absorptionTime Imaging CALorimeter ERC grant, agreement no 338953. The authors would like to acknowledge the support of Dr. Daniel Bonifacio of IPEN, Sao Paolo, Brazil.

## ORCID iDs

G Konstantinou https://orcid.org/0000-0002-1005-282X
A J Gonzalez https://orcid.org/0000-0001-6742-5626

## References

Binder T, Kang H G, Nitta M, Schneider F, Yamaya T, Parodi K and Thirolf P G 2021 Performance evaluation of a staggered three-layer DOI PET detector using a 1 mm LYSO pitch with PETsys TOFPET2 ASIC: comparison of hamamatsu and ketek SiPMs *Phys. Med. Biol.* **66** 125016

Capasso M, Acerbi F, Borghi G, Ficorella A, Furlan N, Mazzi A and Gola A 2020 FBK VUV-sensitive silicon photomultipliers for cryogenic temperatures *Nucl. Instrum. Methods Phys. Res. A* **982** 164478

Carlier T *et al* 2020 'From a PMT-based to a SiPM-based PET system: a study to define matched acquisition/reconstruction parameters and NEMA performance of the Biograph Vision 450' *Ejnmmi Phys.* **7** 55

Gómez S, Alozy J, Campbell M, Fernandez-Tenllado J M, Manera R, Mauricio J and Gascon D 2022 FastIC: a fast integrated circuit for the readout of high performance detectors *J. Instrum.* **17** C05027

Gundacker S, Pots R H, Nepomnyashchikh A, Radzhabov E, Shendrik R, Omelkov S and Auffray E 2021 Vacuum ultraviolet silicon photomultipliers applied to BaF2 cross-luminescence detection for high-rate ultrafast timing applications *Phys. Med. Biol.* **66** 114002

Gundacker S, Turtos R M, Kratochwil N, Pots R H, Paganoni M, Lecoq P and Auffray E 2020 Experimental time resolution limits of modern SiPMs and TOF-PET detectors exploring different scintillators and Cherenkov emission *Phys. Med. Biol.* **65** 025001

Hu C, Zhang L and Zhu R Y 2022 *Inorganic Scintillators for Future HEP Experiments* arXiv:2203.06731

Ieki K, Iwamoto T, Kaneko D, Kobayashi S, Matsuzawa N, Mori T and Yamada R 2019 Large-area MPPC with enhanced VUV sensitivity for liquid xenon scintillation detector. *Nucl. Instrum. Methods Phys. Res.* A **925** 148–55

Jan S *et al* 2004 GATE: a simulation toolkit for PET and SPECT *Phys Med Biol.* **19** 4543–61

Konstantinou G, Barrio J, Moliner L, Cañizares G, Cucarella N, Benlloch J M and Gonzalez A J 2020 A novel metascintillator approach for ultra-fast timing in Positron Emission Tomography *2020 IEEE Nucl. Sci. Symp. Med. Imaging Conf. (NSS/MIC) (Boston, MA, 31 October 2020 – 07 November 2020)* (Picastaway, NJ: IEEE) pp 1–4 IEEE

Konstantinou G, Latella R, Moliner L, Zhang L, Benlloch J M, Lecoq P and Gonzalez A J 2021b Metascintillator pulse feature and shape analysis to detect photoelectric interactions and energy sharing *2020 IEEE Nucl. Sci. Symp. Med. Imaging Conf. (NSS/MIC)* 1–4 IEEE

Konstantinou G, Lecoq P, Benlloch J M and Gonzalez A J 2021a Metascintillators for ultra-fast gamma detectors: a review of current state and future perspectives *IEEE Trans. Radiat. Plasma Med. Sci.* **6** 5–15

Kratochwil N, Gundacker S, Lecoq P and Auffray E 2020 Pushing cherenkov PET with BGO via coincidence time resolution classification and correction *Phys. Med. Biol.* **65** 115004

Latella R, Gonzalez A J, Barrio J, Benlloch J M, Lecoq P and Konstantinou G 2021 Test Setup and Data Selection Protocols for the Measurement of Metascintillator CTR 2021 *IEEE Nucl. Sci. Symp. Med. Imaging Conf. (NSS/MIC)* 1–4 IEEE

Lecoq P 2017 'Pushing the Limits in Time-of-Flight PET Imaging' in *IEEE Trans. Radiat. Plasma Med. Sci.* **1** 473–85

Lecoq P, Konstantinou G, Latella R, Moliner L, Nuyts J, Zhang L and Gonzalez A J 2022 Metascintillators: new results for TOF-PET applications *IEEE Trans. Radiat. Plasma Med. Sci.* **6** 510–6

Lecoq P, Morel C, Prior J O, Visvikis D, Gundacker S, Auffray E and Benoit M 2020 Roadmap toward the 10 ps time-of-flight PET challenge *Phys. Med. Biol.* **65** 21RM01

Loignon-Houle F, Charlebois S A, Fontaine R and Lecomte R 2022 Monte Carlo simulations of energy, time and spatial evolution of primary electrons generated by 511 keV photons in various scintillators *Nucl. Instrum. Methods Phys. Res. A* **1030** 166449

Mao R, Zhang L and Zhu R Y 2011 'LSO/LYSO crystals for future HEP experiments.' Journal of Physics *Conf. Series. Vol. 293. No. 1. IOP Publishing*

Mohr P, Efthimiou N, Pagano F, Kratochwil N, Pizzichemi M, Tsoumpas C and Ziemons K 2022 Image reconstruction analysis for positron emission tomography with heterostructured scintillators *IEEE Trans. Radiat. Plasma Med. Sci.* **7** 41–51

Moliner L, Konstantinou G, Benlloch J M and Lecoq P 2021 Towards TOF improvements: metascintillator simulation using BaF 2 as fast scintillator. In 2021 *IEEE Nucl. Sci. Symp. Med. Imaging Conf. (NSS/MIC)* 1–4 IEEE

Saint G 2021 Crystals datasheet, https://crystals.saint-gobain.com/sites/imdf.crystals.com/files/documents/barium-fluoride-data-sheet.pdf

Zhu R Y 1994 On quality requirements to the barium fluoride crystals *Nucl. Instrum. Methods Phys. Res., Sect. A* **340** 442–57